Available online at www.sciencedirect.com
ScienceDirect
International Journal of Heat and Mass Transfer 51 (2008) 4260–4275
International Journal of HEAT and MASS TRANSFER
www.elsevier.com/locate/ijhmt

Steady-state conjugate natural convection in a fluid-saturated porous cavity

Abdalla Al-Amiri [a], Khalil Khanafer [b], Ioan Pop [c,*]

[a] Mechanical Engineering Department, United Arab Emirates University, United Arab Emirates
[b] Biomedical Engineering Department, University of Michigan, Ann Arbor, MI 48109, USA
[c] Faculty of Mathematics, University of Cluj, R-3400 Cluj, Romania

Received 16 July 2007
Available online 24 March 2008

Abstract

The current numerical investigation addresses the wall heat conduction effect on the natural-convection heat transfer within a two-dimensional cavity, which is filled with a fluid-saturated porous medium. The problem configuration consists of two insulated horizontal walls of finite thickness and two vertical walls which are maintained at constant but different temperatures. The generalized model of the momentum equation, which is also known as the Forchheimer–Brinkman-extended Darcy model, is used in representing the fluid motion inside the porous cavity. The local thermal equilibrium condition is assumed to be valid for the range of the thermophysical parameters considered in the present investigation. The steady-state solution is sought from the undergoing investigation. The momentum and energy transport processes within the porous cavity is examined through depicting the streamlines and isotherms for different domains of a selected dimensionless groups. These dimensionless groups and their respective domains are as follows: $W = 0.0075$–0.2, $K_r = 1$–10, $k_s/k_f = 0.1$–100, $Ra = 10^4$–10^6, $Da = 10^{-5}$–10^{-1}, $\varepsilon = 0.25$–0.95 and $AR = 0.25$–2. The significance of varying these parameters on the predicated average Nusselt number is highlighted and discussed. Finally, the investigation is concluded by presenting the sensitivity of the interface temperature upon varying the above dimensionless groups.

1. Introduction

The phenomenon of convective heat transfer in a fluid-saturated porous medium has received considerable attention due to its relevance in various applications such as biomedical engineering applications, drying processes, thermal insulation, radioactive waste management, transpiration cooling, geophysical systems and contaminant transport in groundwater [1–7]. Comprehensive reviews of the existing studies on these topics can be found in recent monographs by Nield and Bejan [8], Vafai [9], AlAmiri [10], Ingham and Pop [11,12], and Pop and Ingham [13]. Conjugate natural convection in enclosures where heat conduction in a solid wall of finite thickness is coupled with heat convection in an adjacent fluid has been studied extensively in the literature [14–19]. Kim and Viskanta [14,15] analyzed experimentally and numerically the effects of wall conductance on natural convection in square enclosures. They found that heat conduction along the conducting adiabatic walls simultaneously stabilize and destabilize the fluid in the cavity. Meanwhile, conjugate natural convection in enclosures filled with porous media has received less attention. This type of configuration is of interest in several engineering applications. In particular, the solidification process in porous media and building insulation layers.

Most of the studies available in the literature on natural convection in enclosures filled with porous media considered vertical or horizontal layers heated isothermally [20–22]. This assumption is not adequate in many engineering applications. The analysis of natural-convection–conduction heat transfer in a square enclosure filled with porous media and adjacent to a wall of finite thickness is of

* Corresponding author. Tel.: +40 264 594 315; fax: +40 264 591 906.
E-mail address: pop.ioan@yahoo.co.uk (I. Pop).

0017-9310/$ - see front matter © 2008 Elsevier Ltd. All rights reserved.
doi:10.1016/j.ijheatmasstransfer.2007.12.026

Nomenclature

AR	aspect ratio, L/H
b	width of the cavity wall
c_p	specific heat at constant pressure
Da	Darcy number, K/H^2
F	Forchheimer constant
g	acceleration due to gravity
Gr	Grashof number, $g\beta\Delta TH^3/\nu^2$
H	height of the cavity
J	unit vector oriented along the pore velocity vector
k	thermal conductivity
K	permeability of the porous medium
K_r	wall-to-fluid thermal conductivity ratio (k_w/k_f)
L	length of the cavity
Nu	local Nusselt number, defined in Eqs. (12) and (13)
$\overline{Nu}$	average Nusselt number, defined in Eq. (14)
p	pressure
P	dimensionless pressure, $p/\rho(g\beta\Delta TH)$
Pr	Prandtl number, ν/α
Q	total heat transfer
Ra	Rayleigh number, $Gr \cdot Pr$
t	time
T	temperature
T_C	temperature of the cold wall
T_H	temperature of the hot wall
$\mathbf{v}$	dimensional velocity vector
$\boldsymbol{V}$	dimensionless velocity vector, $\mathbf{v}/\sqrt{g\beta\Delta TH}$
W	dimensionless width of the wall, b/H
x	x-coordinate
X	dimensionless X-coordinate, x/H
y	y-coordinate
Y	dimensionless Y-coordinate, y/H

Greek symbols

α	thermal diffusivity
β	coefficient of thermal expansion
ε	porosity of the porous medium
λ	maximum-norm
ν	kinematic viscosity
θ	dimensionless temperature, $(T - T_C)/(T_H - T_C)$
ρ	density
σ	heat capacity ratio, $\lfloor\varepsilon(\rho c_p)_f + (1-\varepsilon)(\rho c_p)_s\rfloor/(\rho c_p)_f$
τ	dimensionless time, $t\sqrt{g\beta\Delta TH}/H$

Subscripts

cond	conduction
eff	effective
f	fluid
porous	porous medium
s	solid
w	wall

practical importance to gain insight on the influence of the existing coupling between walls and fluid-saturated porous media on the fluid flow and heat transfer characteristics [23–25]. Saeid [23,24] studied numerically steady conjugate natural-convection in a two-dimensional porous enclosure with finite wall thickness using the Darcy model. The outcome was presented for various magnitudes of Rayleigh numbers, wall thickness, wall-to-fluid thermal conductivity ratio and the ratio of the solid-to-fluid thermal conductivity of the porous medium. The results illustrated that the average Nusselt number increased with an increase in Rayleigh number and a reduced wall thickness. Furthermore, numerical study of steady-state conjugate natural convection in a square porous cavity with horizontal walls of finite thickness and isothermal vertical walls was studied by Baytas et al. [25] using Darcy–Boussinesq approximation. Their results indicated that the flow characteristics within the enclosure were significantly influenced by the coupling effect between walls and fluid-saturated porous medium. Moreover, Mbaye et al. [26] studied both analytically and numerically natural-convection heat transfer in an inclined porous layer boarded by a wall of a finite thickness and thermal conductivity value. A constant heat flux was applied for heating and cooling the long sidewalls of the rectangular enclosure while the other two walls were kept insulated. The governing equations, derived from the Brinkman-extended Darcy formulation, were solved analytically, in the limit of a thin system, using the parallel flow approximation. In addition, Kimura et al. [27] presented a review of conduction–convection conjugated natural convection in a fluid-saturated porous medium using different configurations such as slender bodies, rectangular slabs, horizontal cylinders and spheres.

The prime objective of the current numerical investigation is to appraise the momentum and energy transport phenomena in a porous cavity boarder by a wall of a finite thickness from one side. The vertical walls were subjected to a temperature gradient while the horizontal walls were kept insulated. It is worth noting that the majority of the reviewed studies on conjugate natural convection in porous media were based on Darcy's law, which silences the inertia and viscous effects on fluid flow and heat transfer. Since the rigid matrix resistance in a porous structure deviates from Darcy's law at high velocities, a generalized flow model (also known as the Brinkman–Forchheimer-extended Darcy model) was utilized in the present investigation to better analyze the transport processes in the presence of the coupling effect between the wall and the fluid-saturated porous medium. The investigation incorporates several pertinent dimensionless groups in conducting the analyses.

These groups are the dimensionless wall thickness, wall-to-fluid thermal conductivity ratio, the porous medium solid-to-fluid thermal conductivity ratio, Rayleigh number and the physical aspect ratio of the cavity.

2. Mathematical formulation

The problem under investigation is a laminar two-dimensional conjugate natural heat transfer convection in a cavity filled with a porous medium. The physical domain under consideration and coordinate system are shown in Fig. 1. The left wall of thickness b is maintained at a constant temperature T_H and the right wall is maintained at a constant temperature T_C, while maintaining $T_H > T_C$. The horizontal walls are assumed to be insulated. In addition, the thermophysical properties of the fluid are assumed constant, except for the density in the buoyancy term in the momentum equations which is treated according to Boussinesq model. Furthermore, the porous medium is considered homogeneous, isotropic and is saturated with a fluid that is in local thermodynamic equilibrium with the solid matrix of the porous medium.

By assimilating the above assumptions, the system of the governing equations can be expressed in canonical forms based on the volume average technique in the porous medium such as [2,28]

Continuity equation:

$$\nabla \cdot \langle \boldsymbol{V} \rangle = 0. \tag{1}$$

Momentum equation:

$$\frac{1}{\varepsilon}\left[\frac{\partial \langle \boldsymbol{V} \rangle}{\partial \tau} + \langle (\boldsymbol{V}\cdot\nabla)\boldsymbol{V} \rangle\right] = -\nabla \langle P \rangle^{\mathrm{f}} + \frac{1}{\varepsilon\sqrt{Gr}}\nabla^2 \langle \boldsymbol{V} \rangle - \frac{\langle \boldsymbol{V} \rangle}{Da\sqrt{Gr}} - \frac{F\varepsilon}{\sqrt{Da}}[\langle \boldsymbol{V} \rangle \cdot \langle \boldsymbol{V} \rangle]J + \theta. \tag{2}$$

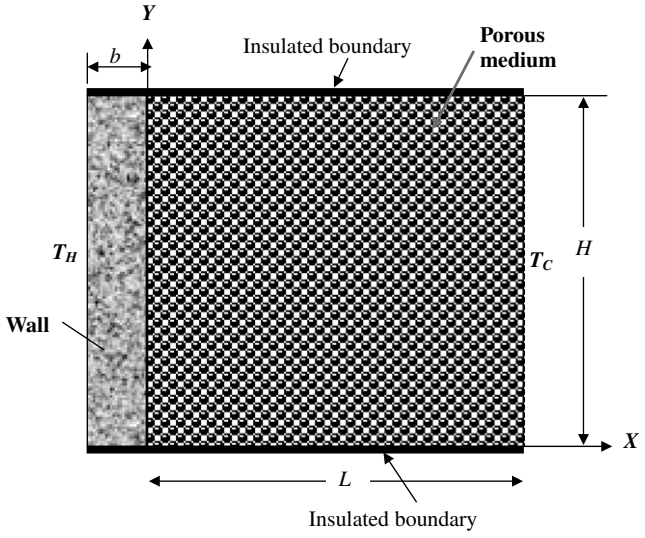

Fig. 1. Schematic diagram of the physical model and coordinate system.

Energy equation:

$$\sigma\frac{\partial \theta}{\partial \tau} + \boldsymbol{V}\cdot\nabla\theta = \frac{k_{\mathrm{eff}}}{k_{\mathrm{f}}}\frac{1}{Pr\sqrt{Gr}}\nabla^2\theta, \tag{3}$$

where

$$k_{\mathrm{eff}} = \varepsilon k_{\mathrm{f}} + (1-\varepsilon)k_{\mathrm{s}} \quad \text{and}$$
$$\sigma = \lfloor \varepsilon(\rho c_p)_{\mathrm{f}} + (1-\varepsilon)(\rho c_p)_{\mathrm{s}} \rfloor / (\rho c_p)_{\mathrm{f}}. \tag{4}$$

Meanwhile, the transport process within the wall can be represented as

$$\nabla^2\theta_{\mathrm{w}} = 0. \tag{5}$$

The above equations were normalized using the following dimensionless parameters:

$$\boldsymbol{V} = \frac{\mathbf{v}}{\sqrt{g\beta\Delta TH}}, \quad P = \frac{p}{\rho(g\beta\Delta TH)},$$
$$\tau = \frac{t\sqrt{g\beta\Delta TH}}{H}, \quad \theta = \frac{T-T_C}{T_H - T_C},$$
$$\mathbf{x} = \frac{(x,y)}{H}, \quad W = \frac{b}{H}, \tag{6}$$

where β is the fluid thermal expansion coefficient, ρ the fluid density, g the gravitational acceleration, P the dimensionless pressure, $\boldsymbol{V}$ the dimensionless velocity vector, $Da = K/KH^2$ the Darcy number and W the dimensionless wall thickness. In addition, the relevant Grashof number and Prandtl number are given by $Gr = g\beta\Delta TH^3/v^2$ and $Pr = v/\alpha$, respectively.

The associated boundary conditions for the problem under consideration can be expressed as

$$X = -W \quad \text{and} \quad 0 \leqslant Y \leqslant 1: \qquad \boldsymbol{V} = 0, \quad \theta_{\mathrm{w}} = 1, \tag{7}$$
$$X = 1 \quad \text{and} \quad 0 \leqslant Y \leqslant 1: \qquad \boldsymbol{V} = \theta = 0,$$

$$Y = 0, 1: \qquad \boldsymbol{V} = \frac{\partial\theta}{\partial Y} = 0. \tag{8}$$

The heat flux equality at the interface ($X = 0$) can be sustained by employing the following condition:

$$k_{\mathrm{eff}}\frac{\partial\theta}{\partial X}\Big)_{\mathrm{porous}} = k_{\mathrm{w}}\frac{\partial\theta_{\mathrm{w}}}{\partial X}\Big)_{\mathrm{solid}}, \tag{9}$$

where k_{w} is the thermal conductivity of the wall. The physical quantities of interest in this investigation are the local Nusselt number and the average Nusselt number, which are, respectively, defined by

$$X = -b: \quad Nu_{\mathrm{w}} = \frac{Q_{\mathrm{wall}}}{Q_{\mathrm{cond}}} = \frac{L}{H}\frac{k_{\mathrm{w}}}{k_{\mathrm{f}}}\left(\frac{\partial\theta_{\mathrm{w}}}{\partial X}\right)_{X=-W} = AR\frac{k_{\mathrm{w}}}{k_{\mathrm{f}}}\left(\frac{\partial\theta_{\mathrm{w}}}{\partial X}\right)_{X=-W}, \tag{10}$$

$$X = 1: \quad Nu_{\mathrm{porous}} = \frac{Q_{\mathrm{porous}}}{Q_{\mathrm{cond}}} = \frac{L}{H}\frac{k_{\mathrm{eff}}}{k_{\mathrm{f}}}\left(\frac{\partial\theta_{\mathrm{porous}}}{\partial X}\right)_{X=1} = AR\frac{k_{\mathrm{eff}}}{k_{\mathrm{f}}}\left(\frac{\partial\theta_{\mathrm{porous}}}{\partial X}\right)_{X=1}, \tag{11}$$

$$\overline{Nu} = \int_0^1 Nu\,\mathrm{d}Y, \tag{12}$$

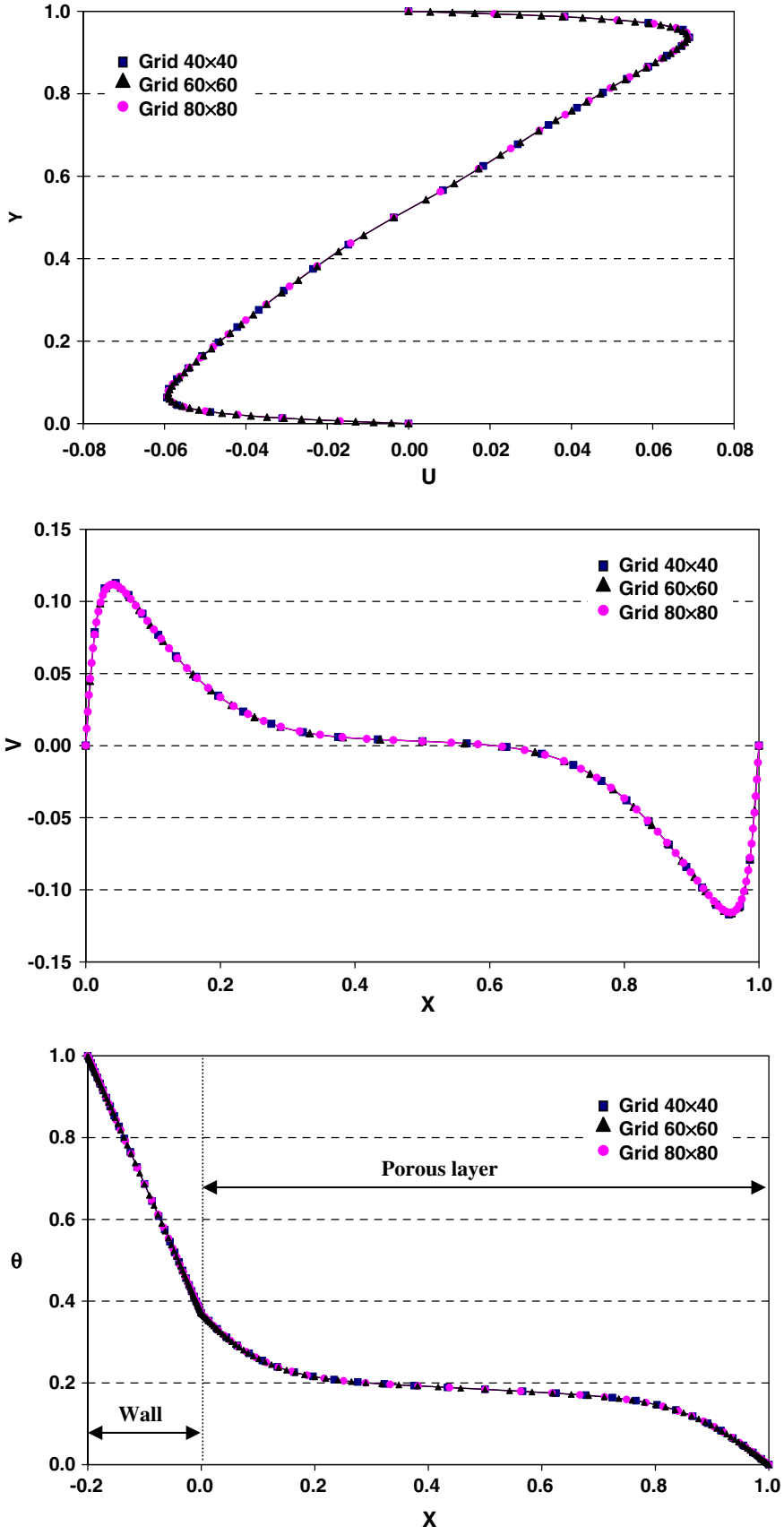

Fig. 2. Velocity and temperature profiles at mid-sections of the cavity for various mesh sizes ($Ra = 10^6$, $Da = 10^{-3}$, $W = 0.2$, $K_r = 5$, $k_s/k_f = 100$).

where $AR = L/H$ is the aspect ratio of the cavity. Both Nusselt number expressions listed in Eqs. (10) and (11) should converge to the same result under steady-state condition.

3. Numerical scheme

A finite element formulation based on the Galerkin method is employed to solve the governing equations. The application of this technique is well documented by Taylor and Hood [29] and Gresho et al. [30]. In the current investigation, the continuum domain is divided into a set of non-overlapping regions called elements. Nine node quadrilateral elements with bi-quadratic interpolation functions are utilized to discretize the physical domain. Moreover, interpolation functions in terms of local normalized element coordinates are implemented to approximate the dependent variables within each element. Subsequently, substitution of the approximations into the system of the governing equations and boundary conditions yields a residual for each of the conservation equations. These residuals are then reduced to zero in a weighted sense over each element volume using Galerkin method.

The highly coupled and non-linear algebraic equations resulting from the discretization of the governing equations are solved using an iterative solution scheme called the segregated-solution algorithm. The advantage of using this method lies in that the global system matrix is decomposed into smaller submatrices and then solved in a sequential manner. This technique results in considerably fewer storage requirements. A pressure projection algorithm is utilized to obtain a solution for the velocity field at every iteration step. Furthermore, the pressure projection version of the segregated algorithm is used to solve the non-linear system. In addition, the conjugate residual scheme is used to solve the symmetric pressure-type equation systems, while the conjugate gradient squared method is used for the non-symmetric advection–diffusion-type equations.

4. Grid refinement

Many numerical experiments of various mesh sizes is performed to attain grid-independent results and to determine the best compromise between accuracy and minimizing computer execution time. As such, a variable grid-size system is employed in the present investigation to capture the rapid changes in the dependent variables especially near the boundaries and the wall–fluid interface where the major

Table 1
Comparison of the average Nusselt number between the present results and other works for various Grashof number and wall-to-fluid conductivity ratio ($K_r = k_w/k_f$)

K_r	$Gr = 10^3$			$Gr = 10^4$			$Gr = 10^5$		
	1	5	10	1	5	10	1	5	10
Present	0.87	1.02	1.04	1.35	1.83	1.92	2.08	3.42	3.72
[16]	0.87	1.02	1.04	–	–	–	2.08	3.42	3.72
[17]	0.87	1.02	1.04	1.35	1.83	1.92	2.08	3.42	3.72
[19]	0.85	1.03	1.04	–	–	–	2.04	3.30	3.60

Table 2
Comparison of the average Nusselt number in a cavity filled with a porous medium between the present results and that of Nithiarasu et al. [31] for various Rayleigh numbers ($\varepsilon = 0.9$, $Da = 10^{-2}$)

Ra	Nu (Present)	Nu [28]	% Error
1×10^3	1.018	1.023	0.49
1×10^4	1.632	1.64	0.49
1×10^5	3.95	3.91	1.02
5×10^5	6.69	6.70	0.15

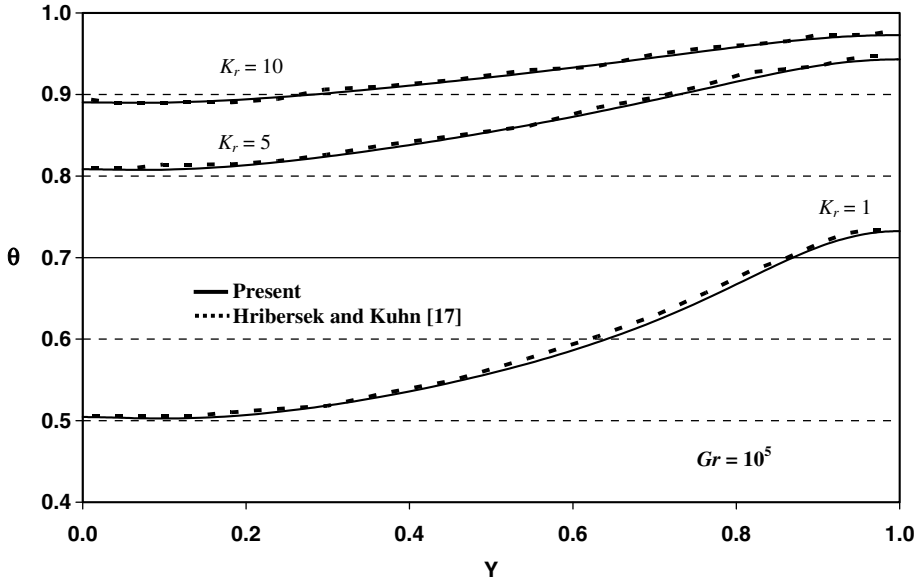

Fig. 3. Comparison of the interface temperature distribution between the present results and Hribersek and Kuhn [17].

gradients occur inside the boundary layer. To test and assess grid independence of the solution scheme, numerical experiments were performed as shown in Fig. 2 for $Ra = 10^6$ using 40×40, 60×60 and 80×80 grid nodes in the porous region, respectively. The results are almost the same even with the relatively coarser grid and this is due to the special arrangement used for the grid nodes (i.e., non-uniform spacing), which renders good results even for relatively coarse grids. In the undergoing investigation, a grid of 80×80 nodes was incorporated for the porous region.

The transient solution is advanced with a time step of 10^{-3} until steady-state solution is obtained. The steady-state solution was assumed to be converged when the var-

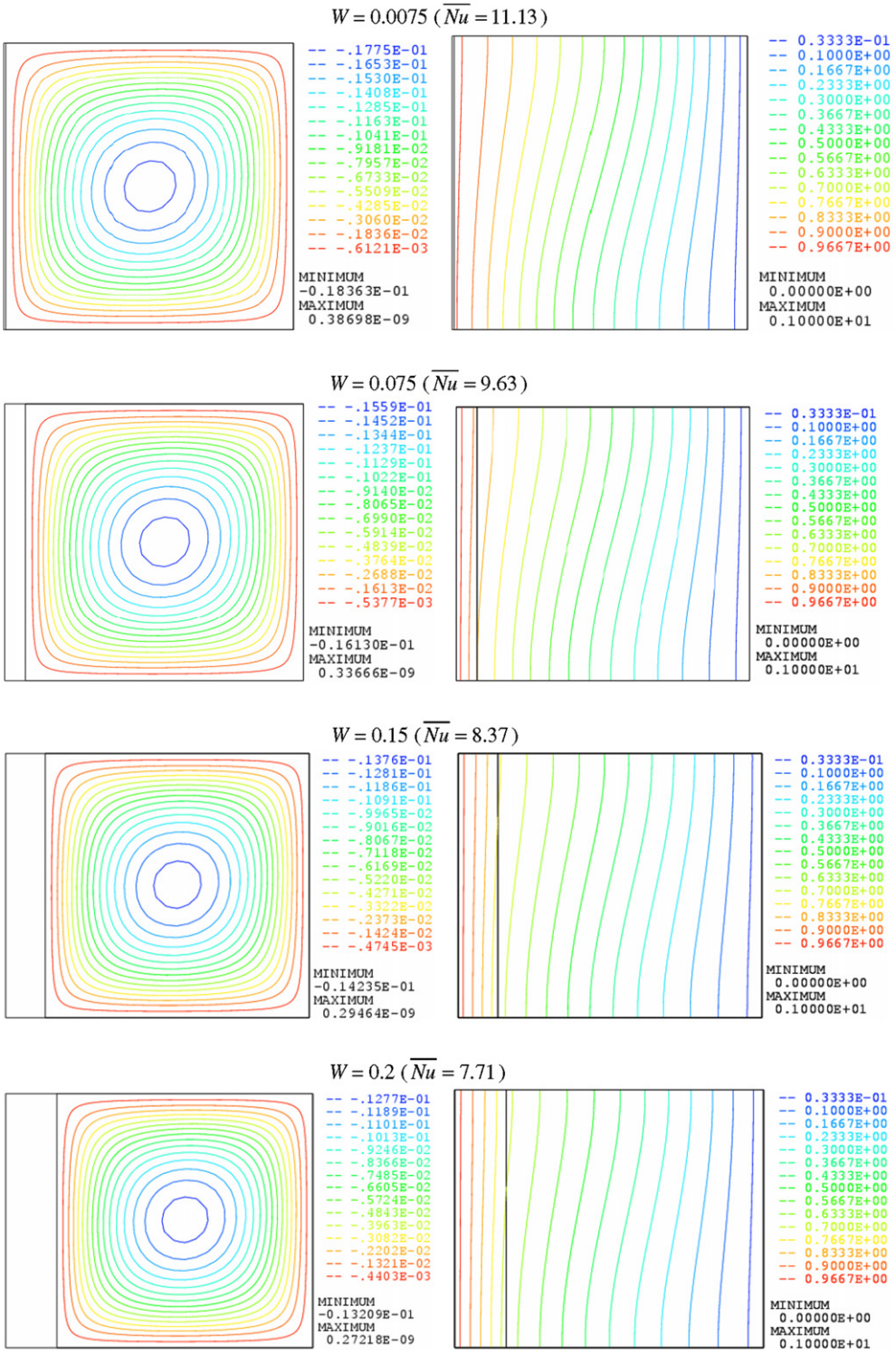

Fig. 4. Effect of varying wall thickness on the streamlines and isotherms using $K_r = 5$, $k_s/k_f = 100$, $Da = 10^{-3}$ and $Gr = 10^5$.

iation of the average Nusselt number between two consecutive time steps is less than 0.1%. An additional check on the convergence to reach a steady-state solution, the standard relative error based on the maximum-norm (λ) was used:

$$\lambda = \frac{\|V^{n+1} - V^n\|_\infty}{\|V^{n+1}\|_\infty} + \frac{\|\theta^{n+1} - \theta^n\|_\infty}{\|\theta^{n+1}\|_\infty} \leqslant 10^{-6}, \quad (13)$$

where the operator $\| \|_\infty$ indicates the maximum absolute value of the variable over all the grid points in the computational domain.

5. Validation

The present numerical code was validated against the benchmark problem of conjugate natural convection in a square cavity with a conducting side wall. The cavity was heated at the left wall and cooled at the right side while the rest of the boundaries were insulated. Table 1 documents the comparison of the average Nusselt number between the outcome of the present code and the available results found in the literature for various Grashof numbers and thermal conductivity ratios. The comparison was in excellent agreement with the results reported by Kaminski and Prakash [16] and Hribersekm and Kuhn [17]. Furthermore, the impact of the wall-to-fluid thermal conductivity ratio ($K_r = k_w/k_f$) on the wall–fluid interface temperatures is illustrated in Fig. 3. Fig. 3 shows that both results are in excellent agreement. An additional verification on the accuracy of the present numerical code is displayed in Table 2, which demonstrates a comparison of the average Nusselt number between the present results and the numerical results of Nithiarasu et al. [31] using the generalized momentum equation of porous medium. The comparisons reveal excellent agreement with the reported studies.

6. Results and discussion

The steady-state results presented in this work are generated for different pertinent dimensionless groups: Rayleigh number ($Ra = 10^3$–10^7), wall-to-fluid thermal conductivity ratio ($K_r = k_w/k_f = 0.01$–10), wall thickness ($W = 0.0075$–0.2), solid-to-fluid thermal conductivity ratio ($k_s/k_f = 1$–100), Darcy number ($Da = 10^{-5}$–10^{-1}), porosity ($\varepsilon = 0.25$–0.95), and aspect ratio ($AR = 0.25$–2). The default parameters are assigned values of $AR = 1$, $W = 0.2$, $K_r = 5$, $k_s/k_f = 100$, $\varepsilon = 0.9$, $Da = 10^{-3}$, $Pr = 1$, and $Gr = 10^5$ unless otherwise stated. The predicted field variables are presented in terms of the streamlines, isotherms and average Nusselt number.

6.1. Effect of wall thickness (W)

The dimensionless wall thickness is defined as $W = b/H$. The effect of wall thickness on the fluid motion and isotherms within the cavity is depicted in Fig. 4. The following parameters were fixed to silence their effects: $K_r = 5$, $k_s/k_f = 100$ and $Gr = 10^5$. The flow circulation in the porous medium is clockwise with a flow upward along the hot left wall and downward at the left cold wall. Further, a central vortex appears as the dominant characteristic of the flow for all the considered values of the dimensionless wall thickness. It can be observed from the isotherm contours that conduction heat transfer regime is manifested in the wall while the convection contribution to the overall energy transport is vivid in the porous cavity. As the wall thickness increases, the strength of the circulation within the porous layer decreases. This is due to the fact that, with the increase in wall thickness, the effective temperature difference that sets up the flow in the porous medium, decreases and the flow strength also diminishes. This can be observed

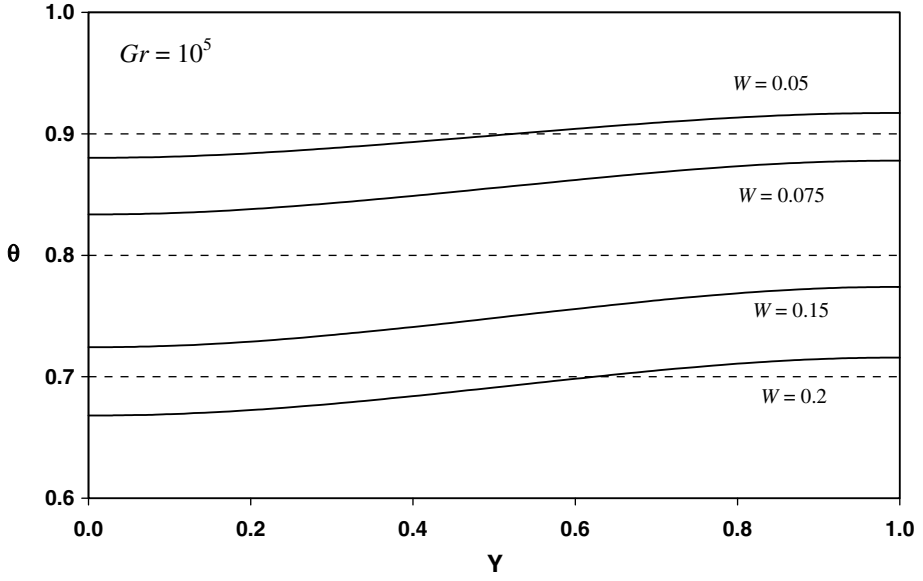

Fig. 5. Temperature distribution at the wall–porous interface for different wall thickness using $K_r = 5$, $Da = 10^{-3}$ and $k_s/k_f = 100$.

by the change in the isotherms strengths within the porous medium with the increase in the wall thickness. Apparently, such a trend impacts the average Nusselt number predictions which tend to decline with the increase in wall thickness (the value of the average Nusselt number is between parentheses for each case in Fig. 4). This is attributed to the fact that, with an increase in the wall thickness, the temperature difference between the solid–porous interface and the cold boundary (i.e., right wall) decreases as illustrated in Fig. 5 and, thus, reducing the magnitude of the average Nusselt number.

It is worth mentioning that the temperature at the interface increases vertically along the wall and this is associated with a fact that the clockwise rotating fluid carries energy from the left wall and, consequently, becomes hot as it rises up against the interface. On the contrary, as the fluid flows

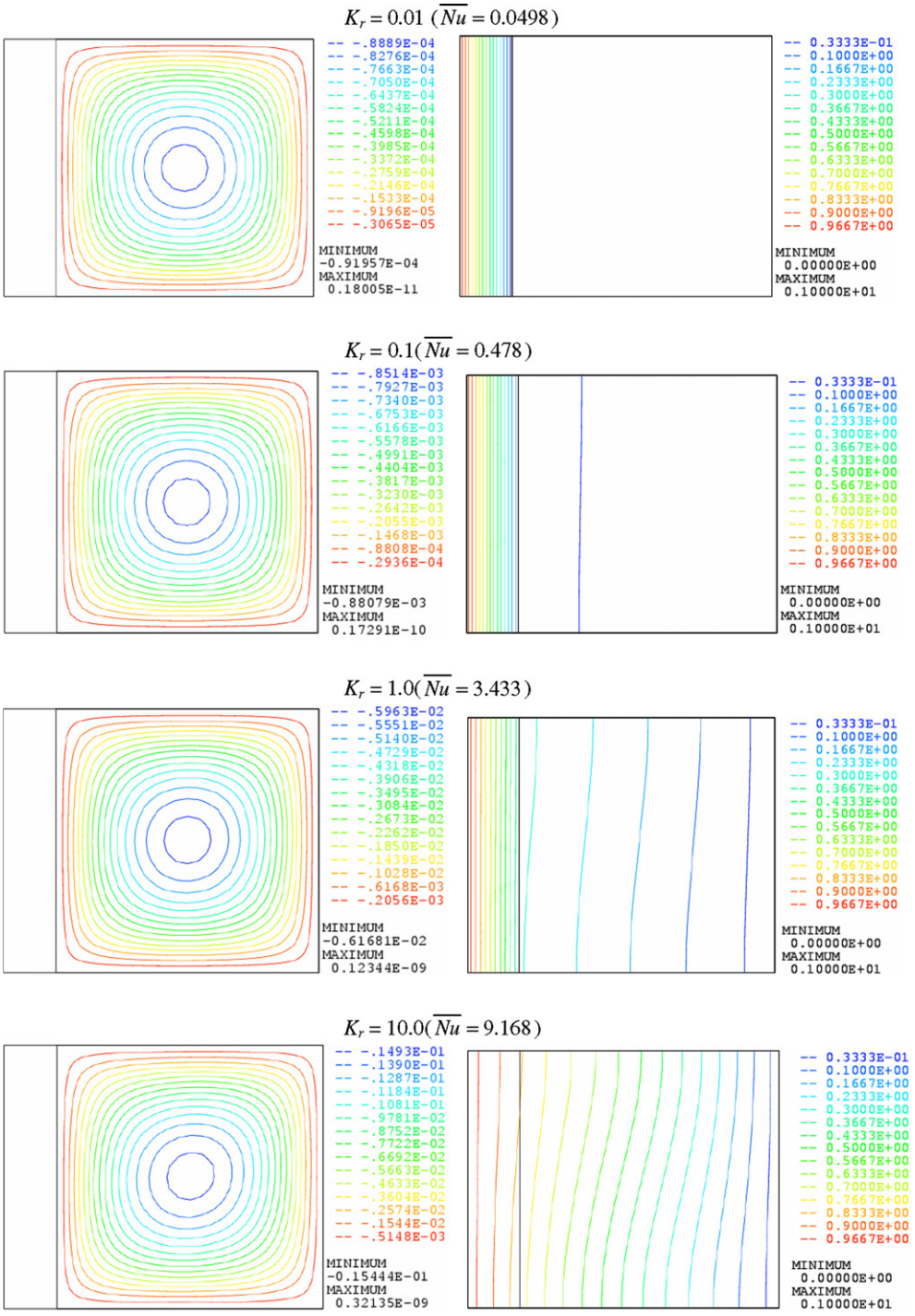

Fig. 6. Effect of varying wall-to-fluid thermal conductivity ratio on streamlines and isotherms using $W = 0.2$, $k_s/k_f = 100$, $Da = 10^{-3}$ and $Gr = 10^5$.

downward along the cold wall, its temperature decreases gradually which is reflected on the interface temperature at $Y = 0$.

6.2. Effect of wall-to-fluid thermal conductivity ratio (K_r)

Fig. 6 demonstrates that the wall-to-fluid thermal conductivity ratio has a significant effect on the streamlines and isotherms. The following parameters were kept constants: $AR = 1$, $W = 0.2$, $k_s/k_f = 100$ and $Gr = 10^5$. For poorly conducting wall scenarios, i.e., $K_r = 0.01, 0.1$, the results merely render a conduction heat transfer regime as vivid from the one-dimensional wall conduction pattern. In addition, the results shown in Fig. 6 signals that natural convection inside the porous medium has totally diminished as manifested from the streamlines values, which are driven by the temperature difference between the interface and the cold boundary. Therefore, the temperature within the porous medium is almost uniform and equal to the cold boundary temperature for poorly conducting wall. As K_r increases from 1 to 10, it can be observed that the intensity of circulation within the porous medium intensifies. This is due to the increase in the sustained temperature difference between the solid–porous interface temperature and the cold boundary increases as a result of an increase in K_r magnitude. Moreover, the isotherms are observed to depart from its vertical pattern in the cavity which indicates that the heat transfer mechanism has changed from a dominant conduction heat transfer regime to encompass convection heat transfer. Thus, the contribution of the natural-convection heat transfer to the overall energy transport mechanism increases with the increase in the wall-to-fluid thermal conductivity ratio.

Fig. 6 illustrates the effect of the wall-to-fluid thermal conductivity ratio on the average Nusselt number predications. The value of the average Nusselt number is between parentheses for each case in Fig. 6. The average Nusselt number is found to increase with an increase K_r magnitude. This is a logical result since increasing the thermal conductivity of the wall will decrease the thermal resistance of the system under consideration. Accordingly, this will increase the strength of convection intensity in the cavity, and hence, enhances the Nusselt number results. Fig. 7 shows the variation of solid–porous interface temperature for different values of wall-to-fluid thermal conductivity ratio. When considering low K_r values such as 0.01 and 0.1, the wall behaves as an insulating layer. As a result, the interface temperature becomes almost identical to the cold boundary temperature. For a high K_r value, however, the conjugate wall becomes very much conductive, which brings about an appreciated increase in the interface temperature resulting in heat transfer augmentation within the cavity.

6.3. Effect of the porous medium solid-to-fluid thermal conductivity ratio (k_s/k_f)

The effect of varying the porous medium solid-to-fluid thermal conductivity on streamlines and isotherms is presented in Fig. 8 for a square cavity, i.e., $AR = 1$. It can be noted from Fig. 8 that the central vortex is elliptic in shape for low k_s/k_f values. It is apparent that as the conductivity ratio increases, the porous medium becomes more conductive causing the central vortex becomes nearly circular. Further, the isotherms within the porous medium are observed to pursue a less two-dimensional pattern with the increase in k_s/k_f value, which signals that the conduction heat transfer regime is dominating the overall energy transport process within the porous cavity. In addition, Fig. 9 illustrates the implications of varying k_s/k_f on the average Nusselt number and the average interface temperature. The overall heat transfer rate increases almost line-

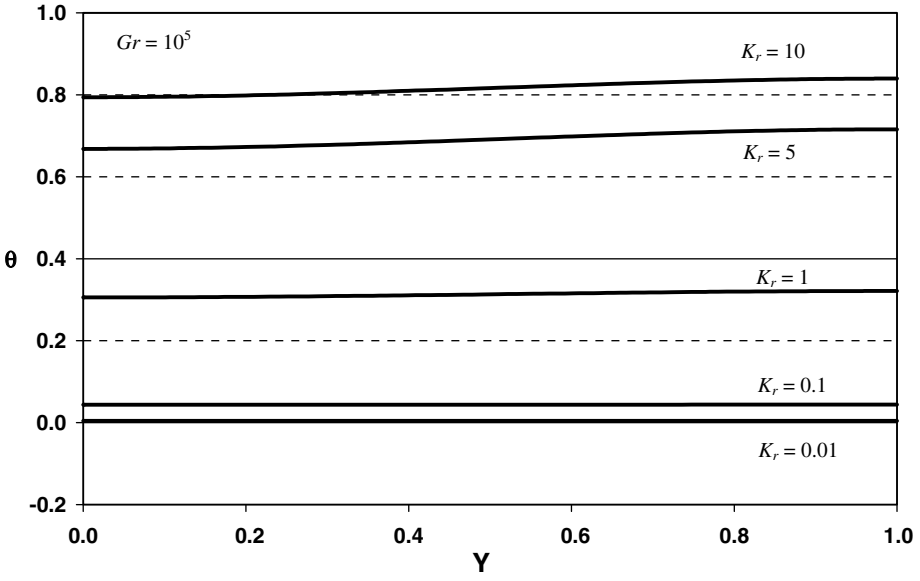

Fig. 7. Temperature distribution at the solid–porous interface for different wall thermal conductivity ratio using $W = 0.2$, $Da = 10^{-3}$ and $k_s/k_f = 100$.

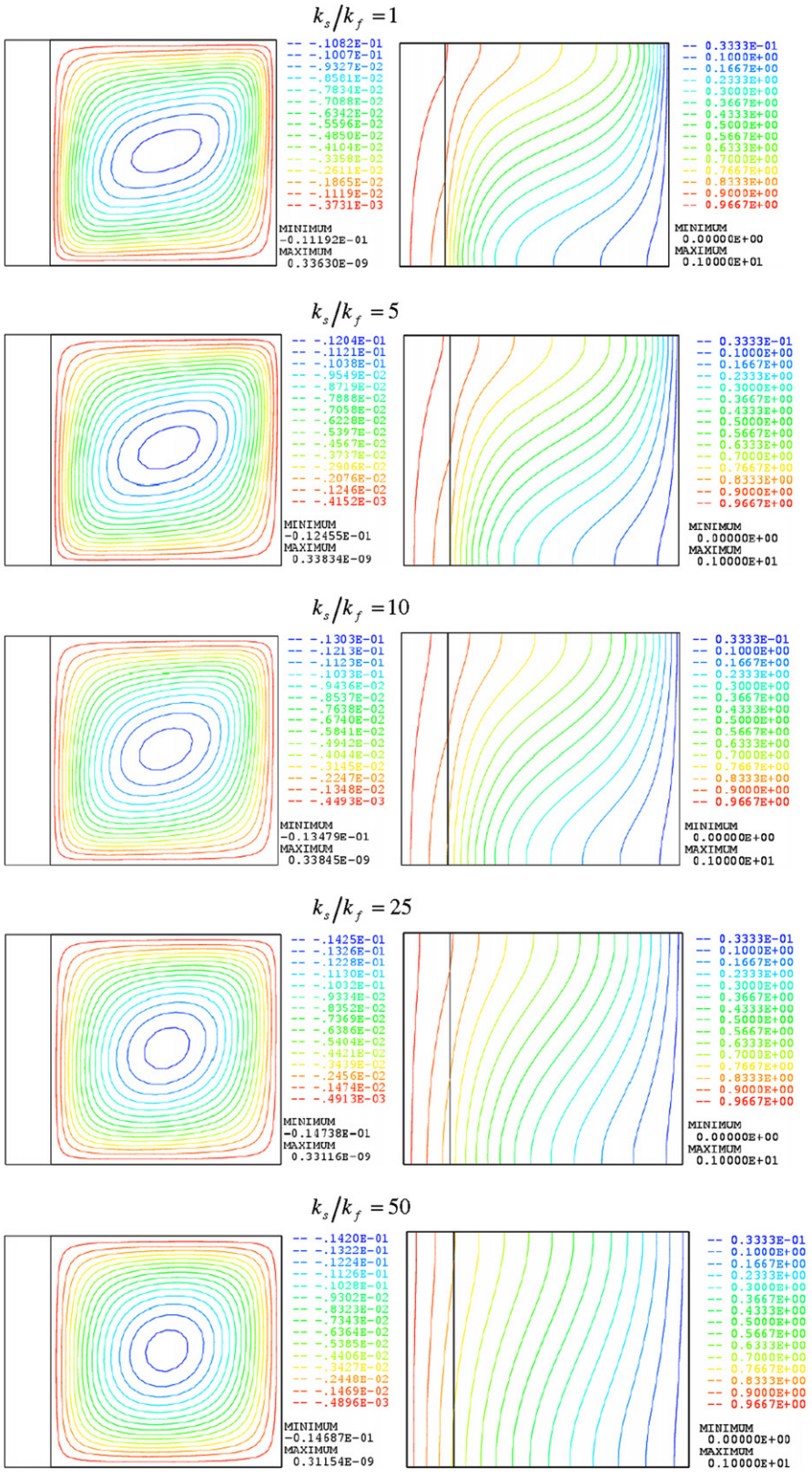

Fig. 8. Effect of varying the porous medium thermal conductivity ratio (k_s/k_f) on the streamlines and isotherms using $W = 0.2$, $Da = 10^{-3}$, $K_r = 5$ and $Gr = 10^5$.

arly with an increase in the thermal conductivity ratio. When increasing the k_s/k_f value from 20 to 100, for example, the average Nusselt number is found to increase by 2.1 folds. Furthermore, it is worth noting that the porous medium becomes very much conductive as k_s/k_f increases. Such an observation is particularly vivid at $k_s/k_f = 100$. This

subsequently causes the average interface temperature and the spatial variation of the interface temperature to decrease with the increase in k_s/k_f value as displayed in Figs. 9 and 10. The results presented in Figs. 8–10 demonstrate an interesting observation, which up to the authors' knowledge were not reported previously in the literature. In referring back to Fig. 8, it exhibits that the flow activities intensify as the thermal conductivity increases for $k_s/k_f \leqslant 25$. When considering $k_s k_f \geqslant 50$, however, flow activities deteriorate and this is associated with a decrease in the average interface temperature, which is considered the driving mechanism for natural convection within the porous cavity. Although the average interface temperature decreases as k_s/k_f increases, the average Nusselt number is found to increase as displayed in Fig. 9. Needless to say, the average Nusselt number is the product of the effective thermal conductivity of the porous medium, which is a function of k_s/k_f, and the temperature gradient between the interface and the cold wall. Hence, despite the depreciation in the temperature gradient which hinders flow activities within the porous medium when considering larger values of k_s/k_f, the attained Nusselt number prediction improves

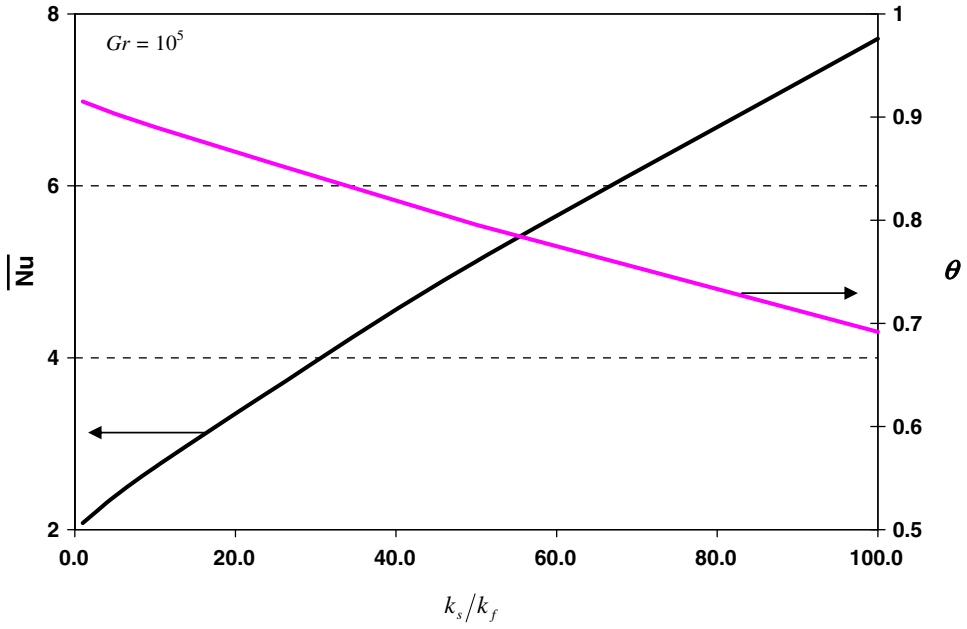

Fig. 9. Effect of varying the porous medium thermal conductivity (k_s/k_f) on the average Nusselt number and average interface temperature using $W = 0.2$, $Da = 10^{-3}$ and $K_r = 5$.

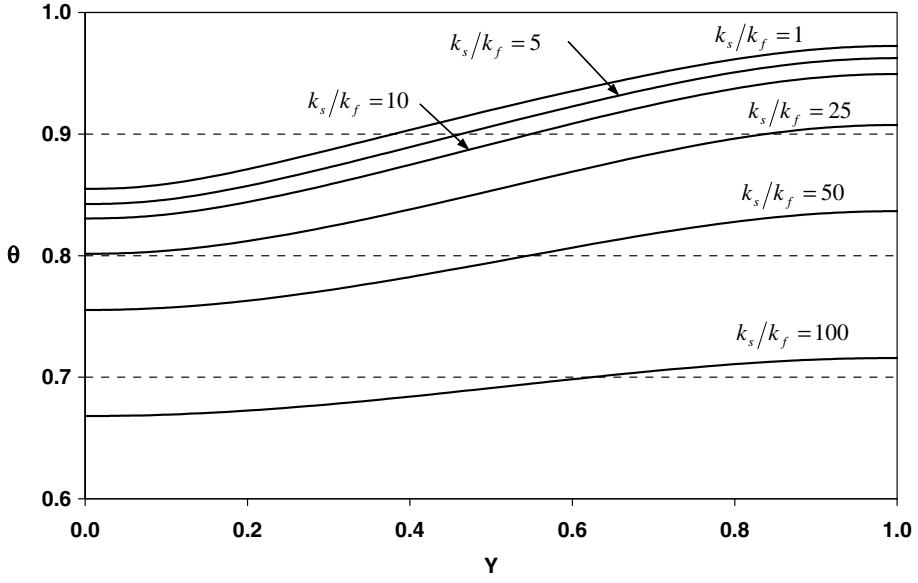

Fig. 10. Temperature distribution at the solid–porous interface for different porous (k_s/k_f) values using $W = 0.2$, $Da = 10^{-3}$ and $K_r = 5$.

since it is a function of the product of k_s/k_f and the temperature gradient between the interface and the cold wall.

6.4. Effect of Rayleigh number (Ra)

The effect of Rayleigh number on the streamlines and isotherms is shown in Fig. 11 using $AR = 1$, $W = 0.2$, $K_r = 5$ and $k_s/k_f = 100$. For low Rayleigh number values, the streamlines are characterized by a single main vortex with that occupies the entire cavity body. The corresponding isotherms are mostly parallel to the vertical walls, which signal that most of the heat transfer is performed by conduction. The contribution of convection is noticeable at high Rayleigh numbers as evident by the departure of the isotherms from the vertical pattern. As Rayleigh number increases is elevated to $Ra = 10^6$, the central vortex becomes distorted into an elliptic shape and the presence of convection becomes more pronounced. This is likely asso-

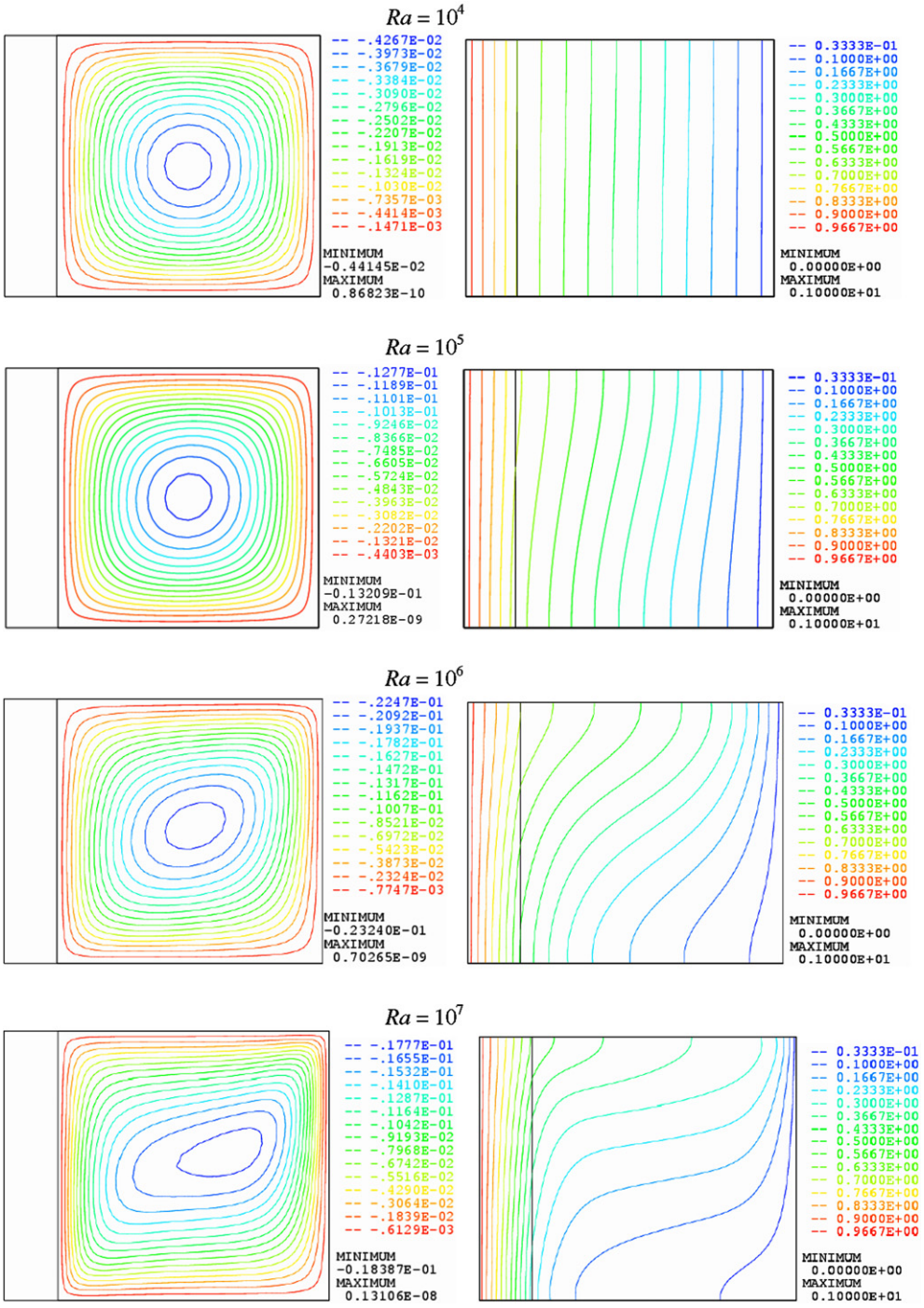

Fig. 11. Effect of varying the Rayleigh number on the streamlines and isotherms using $W = 0.2$, $K_r = 5$, $Da = 10^{-3}$ and $k_s/k_f = 100$.

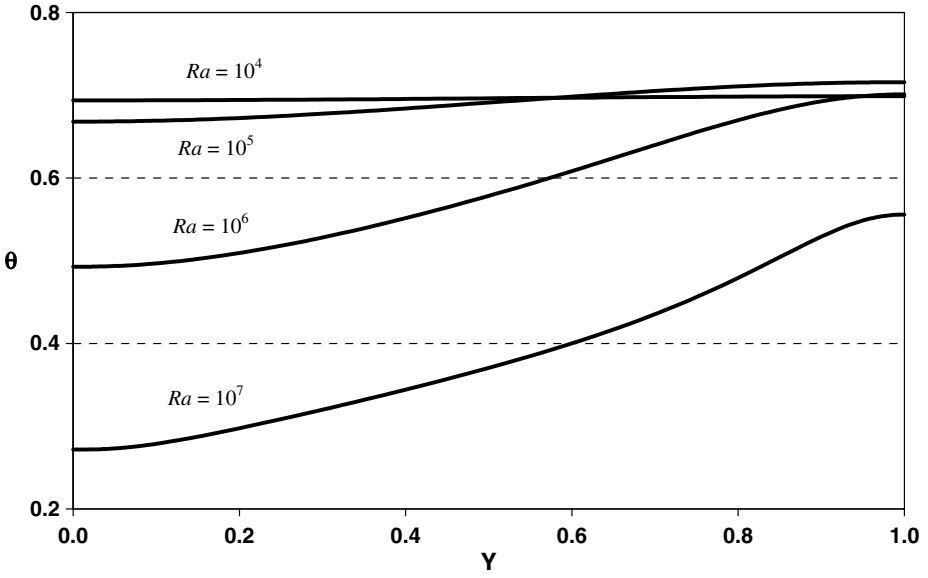

Fig. 12. Temperature distribution at the solid–porous interface for different Rayleigh numbers using $W = 0.2$, $K_r = 5$, $Da = 10^{-3}$ and $k_s/k_f = 100$.

ciated to the high temperature gradients near the vertical walls. Further increase in Rayleigh number to $Ra = 10^7$ causes the central vortex to elongate further with its center close to the cold wall. This can be attributed to high convection current within the cavity which also causes a reduction in the temperature gradients in the center of the cavity due to good fluid mixing as shown in Fig. 11. What is more, the impact of Rayleigh number on the interface temperature is presented in Fig. 12. This figure demonstrates that the interface temperature is about uniform for low Rayleigh numbers which indicates that the heat transfer is achieved primarily by conduction. As Rayleigh number increases to $Ra = 10^5$, the intensity of convection within the cavity picks up and, consequently, the average interface temperature decreases with an increase in Rayleigh number. Such an observation is further pronounced for $Ra = 10^6$ and $Ra = 10^7$, respectively.

6.5. Effect of aspect ratio ($AR = L/H$)

The effect of the cavity aspect ratio on the streamlines and isotherms is depicted in Fig. 13. The contribution of natural convection can be observed from the isotherm patterns when considering $AR = 2$ and $AR = 1$. As the aspect ratio decreases further, the central vortex of the streamlines elongates in the vertical direction and the intensity of circulation within the porous medium decreases. The buoyancy forces with the cavity depreciate as the fluid is expected to travel a longer vertical distance without an increase in the sustained temperature difference. Such an effect impacts the isotherms, which become more parallel to the vertical wall indicating overwhelmed conduction heat transfer regime especially when using the small aspect ratio (i.e., $AR = 0.25$) considered in this investigation. Moreover, it is observed that as the aspect ratio reduces, the vertical boundary layers of the hot and cold walls approach each other and are positioned to be in better thermal communication with each other. This will reduce the degree of heating and cooling on both wall boundary layers and, hence, drops the overall average Nusselt number as shown between parentheses for each case in Fig. 13.

6.6. Effect of Darcy number and porosity of porous medium

The effect of Darcy number and porosity of porous medium on the average Nusselt number are illustrated in Figs. 14 and 15. For small values of the Darcy numbers, the fluid experiences a pronounced large resistance as it flows through the porous matrix causing the flow to cease in the porous region. This subsequently results in hindering flow activities in the porous region. As the porosity of the porous medium decreases, the average Nusselt number increases as depicted in Fig. 15. This is associated with an increase in the effective thermal conductivity of porous medium as the porosity decreases.

7. Heat transfer correlation

The average Nusselt number is correlated over a wide range of various pertinent dimensionless groups employed in this investigation, such as the Rayleigh number $Ra = 10^3$–10^7, wall thickness $W = 0.0075$–0.2, wall-to-fluid thermal conductivity ratio $K_r = 1$–10, porous medium thermal conductivity ratio $k_s/k_f = 1$–100, $Da = 10^{-3}$, $\varepsilon = 0.9$, and aspect ratio $AR = 0.25$–2. This correlation can be mathematically expressed as follows:

$$\overline{Nu} = 0.0606(W \times AR)^{-0.1422}(AR \times k_s/k_f)^{0.444}(K_r)^{0.4348}(Ra)^{0.1587}(AR)^{0.0752}, \quad (14)$$

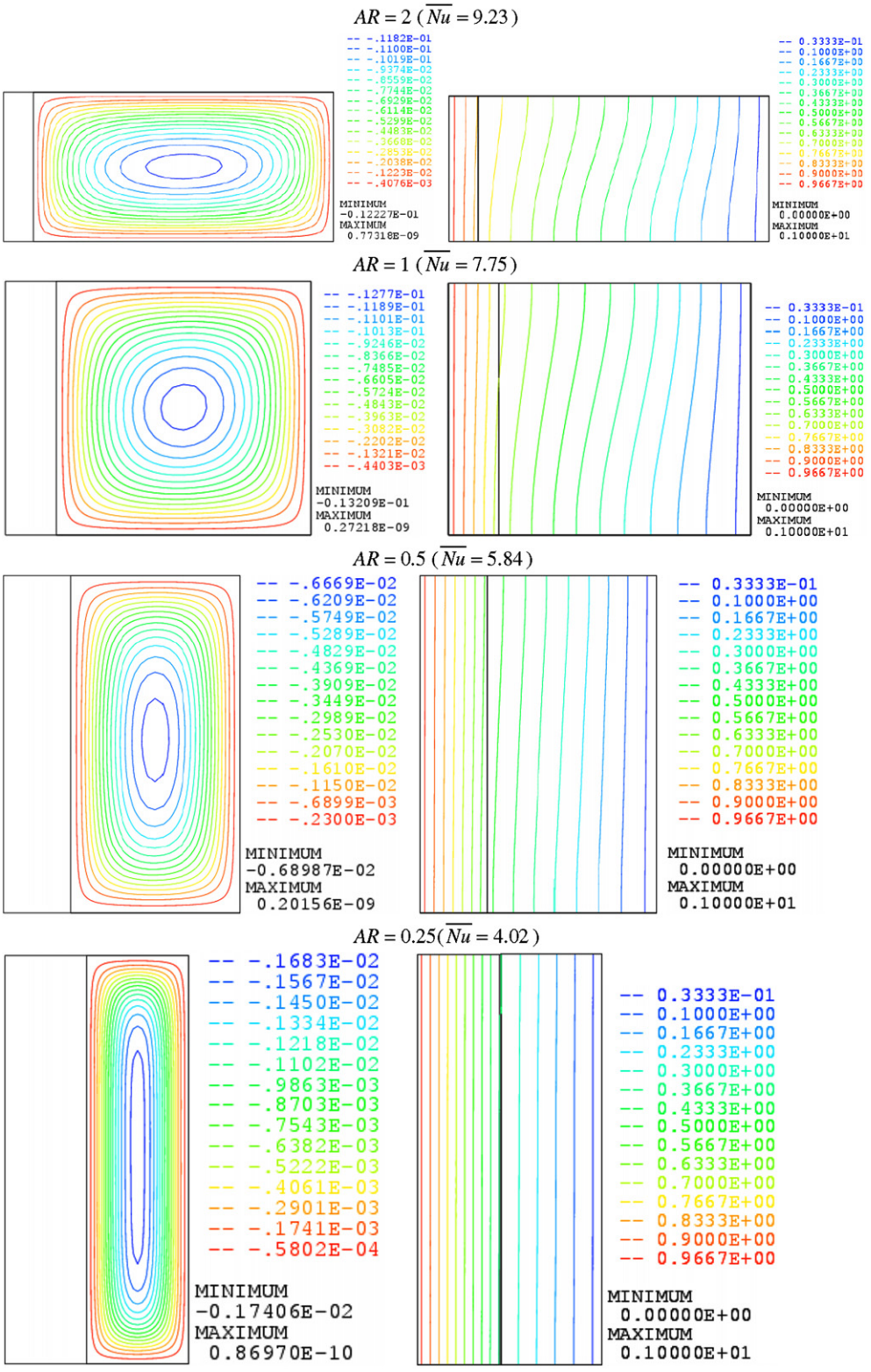

Fig. 13. Effect of varying the aspect ratio on the streamlines and isotherms using $W = 0.2$, $K_r = 5$, $k_s/k_f = 100$, $Da = 10^{-3}$ and $Gr = 10^5$.

where the confidence coefficient for the above equation is $R^2 = 97.8\%$. This correlation reveals that the average Nusselt number value has the strongest dependency on K_r and k_s/k_f, while it has the least dependency on the aspect ratio. Meanwhile, the exponents of the Rayleigh number Ra and the dimensionless wall thickness W are found to be in close proximity. Such an observation is a vital tool when considering designing a configuration with a porous medium and a conjugate wall.

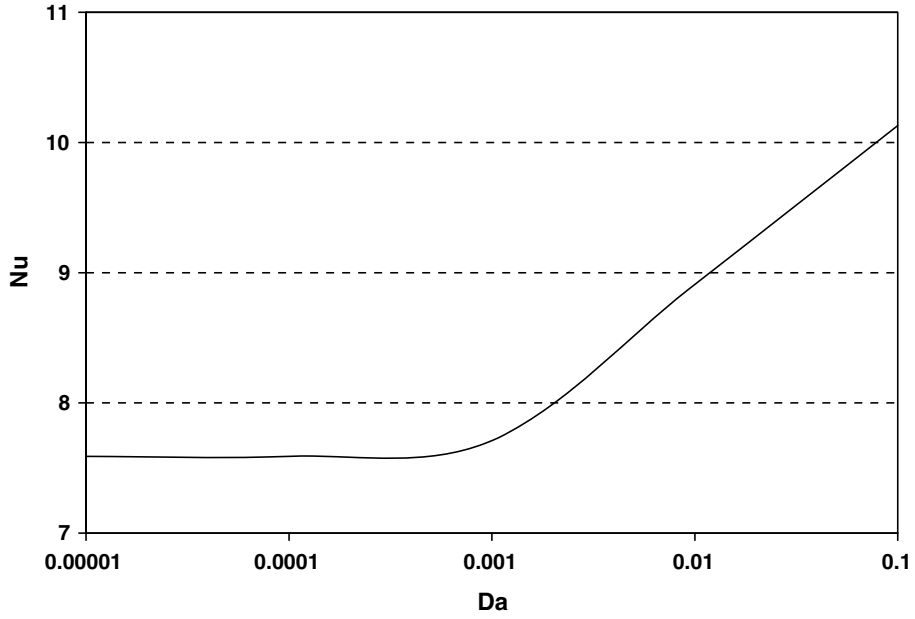

Fig. 14. Effect of Darcy number on the average Nusselt number using $W = 0.2$, $K_r = 5$, $k_s/k_f = 100$ and $Gr = 10^5$.

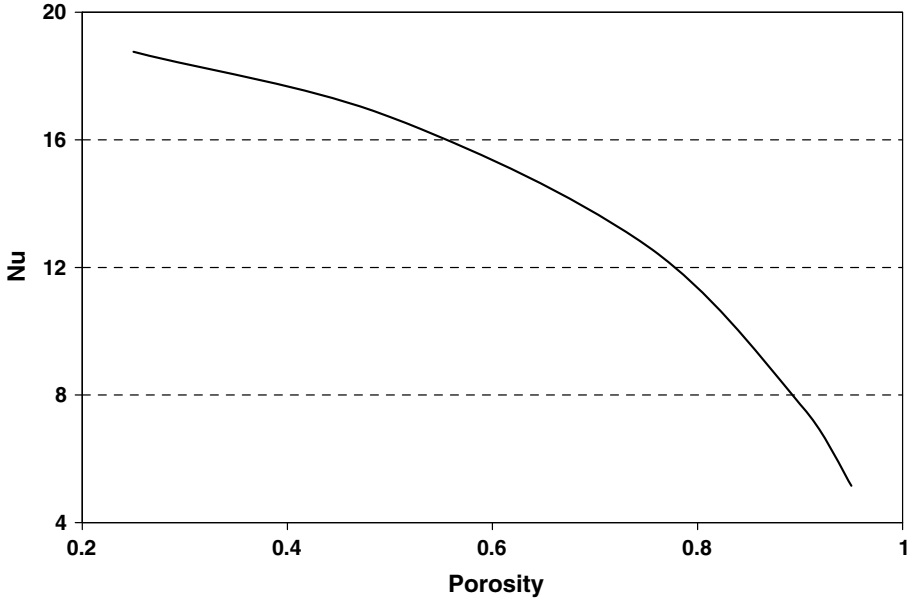

Fig. 15. Effect of porous medium porosity on the average Nusselt number using $W = 0.2$, $K_r = 5$, $k_s/k_f = 100$, $Da = 10^{-3}$ and $Gr = 10^5$.

8. Conclusion

A numerical investigation using finite element method is carried out for steady conjugate natural convection in a fluid-saturated porous cavity boarded to a conducting vertical wall. In this investigation, the fluid motion is predicted using the general formulation of the porous medium, which accounts for the inertial and solid viscous effect. In addition, the momentum and energy transport processes are explored and results of streamlines, isotherms, wall interface temperature and average Nusselt numbers are presented for a wide range of dimensionless parameters. These parameters include the conjugate wall thickness, wall-to-fluid thermal conductivity ratio, solid-to-fluid thermal conductivity of the porous medium, Rayleigh number and aspect ratio. The results showed that as the wall thickness increases, the temperature difference between the interface temperature and the cold boundary reduces, which accordingly brings about a reduction in the overall Nusselt number. However, appreciated increase in the fluid circulation intensity within the porous medium was achieved when considering thin wall thickness, large wall-to-fluid thermal conductivity ratio and large aspect ratio values. The numerical results have indicated that the energy is

primarily transferred by conduction heat transfer in the wall and porous medium for small Rayleigh numbers. Furthermore, predicted average Nusselt number was observed to increase with the increase in the Rayleigh number. Moreover, the higher solid-to-fluid thermal conductivity ratio of the porous medium is found to significantly improve the average Nusselt number. Finally, a Nusselt number correlation was established for a wide range of the considered dimensionless groups in this investigation. The Nusselt number correlation was found to be a strong function of K_r and k_s/k_f, while it was relatively a weak function of the cavity aspect ratio.

References

[1] K. Khanafer, K. Vafai, The role of porous media in biomedical engineering as related to magnetic resonance imaging and drug delivery, Heat Mass Transfer 42 (2006) 939–953.

[2] K. Khanafer, K. Vafai, Isothermal surface production and regulation for high heat flux applications utilizing porous inserts, Int. J. Heat Mass Transfer 44 (2001) 2933–2947.

[3] K. Khanafer, K. Vafai, Double-diffusive mixed convection in a lid driven enclosure filled with a fluid-saturated porous medium, Numer. Heat Transfer: Part A 42 (2002) 465–486.

[4] S.A. Khashan, A.M. AlAmiri, I. Pop, Numerical simulation of natural convection heat transfer in porous cavity heated from below using a non-Darcian and thermal non-equilibrium model, Int. J. Heat Mass Transfer 49 (2006) 1039–1049.

[5] A. Amiri, K. Vafai, Transient analysis of incompressible flow through a packed bed, Int. J. Heat Mass Transfer 41 (1998) 4259–4279.

[6] A. Amiri, K. Vafai, T.M. Kuzay, Effect of boundary conditions on non-Darcian heat transfer through porous media and experimental comparisons, Numer. Heat Transfer: Part A 27 (1995) 651–664.

[7] A. Amiri, K. Vafai, Analysis of dispersion effects and non-thermal equilibrium, non-Darcian, variable porosity, incompressible flow through porous medium, Int. J. Heat Mass Transfer 37 (1994) 939–954.

[8] D.A. Nield, A. Bejan, Convection in Porous Media, second ed., Springer-Verlag, NY, 1995.

[9] K. Vafai, Handbook of Porous Media, second ed., Taylor and Francis Group, NY, 2005.

[10] A. Al-Amiri, Natural convection in porous enclosures: the application of the two-energy equation model, Numer. Heat Transfer: Part A 41 (2002) 817–834.

[11] D.B. Ingham, I. Pop (Eds.), Transport Phenomenon in Porous Media, vol. I, Pergamon, Oxford, 1998.

[12] D.B. Ingham, I. Pop (Eds.), Transport Phenomena in Porous Media, vol. III, Elsevier, Oxford, 2005.

[13] I. Pop, D.B. Ingham, Convective Heat Transfer: Mathematical and Computational Modeling of Viscous Fluids and Porous Media, Pergamon, Oxford, 2001.

[14] D.M. Kim, R. Viskanta, Effect of wall heat conduction on natural convection heat transfer in a square enclosure, J. Heat Transfer 107 (1985) 139–146.

[15] D.M. Kim, R. Viskanta, Study of the effects of wall conductance on natural convection in differently oriented square cavities, J. Fluid Mech. 144 (1984) 153–176.

[16] D.A. Kaminski, C. Prakash, Conjugate natural convection in a square enclosure: effect of conduction in one of the vertical walls, Int. J. Heat Mass Transfer 29 (1986) 1979–1988.

[17] M. Hribersek, G. Kuhn, Conjugate heat transfer by boundary-domain integral method, Eng. Anal. Boundary Elem. 24 (2000) 297–305.

[18] A. Malatip, N. Wansophark, P. Dechaumphai, Combined streamline upwind Petrov Galerkin method and segregated finite element algorithm for conjugate heat transfer problems, J. Mech. Sci. Tech. 20 (2006) 1741–1752.

[19] N. Wansophark, A. Malatip, P. Dechaumphai, Streamline upwind finite element method for conjugate heat transfer problems, Acta Mech. Sinica 21 (2005) 436–443.

[20] V. Prasad, F.A. Kulacki, Convective heat transfer in a rectangular porous cavity – effects of aspect ratio on flow structure and heat transfer, ASME J. Heat Transfer 106 (1984) 158–165.

[21] A. Bejan, D. Poulikakos, The non-Darcy regime for vertical boundary layer convection in a porous medium, Int. J. Heat Mass Transfer 27 (1984) 717–722.

[22] M. Haajizadeh, A.F. Ozguc, C.L. Tien, Natural convection in a vertical porous enclosures with internal heat generation, Int. J. Heat Mass Transfer 27 (1984) 1893–1902.

[23] N. Saeid, Conjugate natural convection in a vertical porous layer sandwiched by finite thickness walls, Int. Commun. Heat Mass Transfer 34 (2007) 210–216.

[24] N. Saeid, Conjugate natural convection in a porous enclosure: effect of conduction in one of the vertical walls, Int. J. Therm. Sci. 46 (2007) 531–539.

[25] A.C. Baytas, A. Liaqat, T. Grosan, I. Pop, Conjugate natural convection in a square porous cavity, Heat Mass Transfer 37 (2001) 467–473.

[26] M. Mbaye, E. Bilgen, P. Vasseur, Natural-convection heat transfer in an inclined porous layer boarded by a finite-thickness wall, Int. J. Heat Fluid Flow 14 (1993) 284–291.

[27] S. Kimura, T. Kiwata, A. Okajima, I. Pop, Conjugate natural convection in porous media, Adv. Water Res. 20 (1997) 111–126.

[28] A. Al-Amiri, Analysis of momentum and energy transfer in a lid-driven cavity filled with a porous medium, Int. J. Heat Mass Transfer 43 (2000) 3513–3527.

[29] C. Taylor, P. Hood, A numerical solution of the Navier–Stokes equations using finite-element technique, Comput. Fluids 1 (1973) 73–89.

[30] P.M. Gresho, R.L. Lee, R.L. Sani, On the time-dependent solution of the incompressible Navier–Stokes equations in two and three dimensions, in: Recent Adv. Numer. Methods in Fluids, Pineridge, Swansea, UK, 1980.

[31] P. Nithiarasu, K.N. Seetharanu, T. Sundararajan, Natural convective heat transfer in a fluid saturated variable porosity medium, Int. J. Heat Mass Transfer 40 (1997) 3955–3967.